



Paper and Salt: Biodegradable NaCl-Based Humidity Sensors for Sustainable Electronics

Aniello Falco¹, Antonio Marín-Sánchez², Florin C. Loghin³, Encarnación Castillo⁴, Alfonso Salinas-Castillo², José F. Salmerón³ and Almudena Rivadeneyra^{4*}

¹Faculty of Science and Technology, Free University of Bolzano-Bozen, Bolzano, Italy, ²Department of Analytical Chemistry, University of Granada, Granada, Spain, ³Institute for Nanoelectronics, Technical University of Munich, Munich, Germany, ⁴Department of Electronics and Computer Technology, University of Granada, Granada, Spain

OPEN ACCESS

Edited by:

Khaled nabil Salama,
King Abdullah University of Science
and Technology, Saudi Arabia

Reviewed by:

Sherjeel Khan,
King Abdullah University of Science
and Technology, Saudi Arabia
Sandeep G. Surya,
Dyson, United Kingdom
Sakandar Rauf,
King Abdullah University of Science
and Technology, Saudi Arabia
Anindya Nag,
King Abdullah University of Science
and Technology, Saudi Arabia

*Correspondence:

Almudena Rivadeneyra
arivadeneyra@ugr.es

Specialty section:

This article was submitted to
Flexible Electronics,
a section of the journal
Frontiers in Electronics

Received: 17 December 2021

Accepted: 02 February 2022

Published: 09 March 2022

Citation:

Falco A, Marín-Sánchez A, Loghin FC,
Castillo E, Salinas-Castillo A,
Salmerón JF and Rivadeneyra A (2022)
Paper and Salt: Biodegradable NaCl-
Based Humidity Sensors for
Sustainable Electronics.
Front. Electron. 3:838472.
doi: 10.3389/felec.2022.838472

Flexible and thin-film humidity sensors are currently attracting the attention of the scientific community due to their portability and reduced size, which are highly useful traits for use in the Internet of Things (IoT) industry. Furthermore, in order to perform efficient and profitable mass production, it is necessary to develop a cost-effective and reproducible fabrication process and materials. Green fabrication methods and biodegradable materials would also minimize the environmental impact and create a sustainable IoT development. In this paper, flexible humidity sensors based on a common salt (NaCl) sensing layer are reported. Our sensors and the fabrication techniques employed, such as dip and spray coating, provide a biodegradable, low cost, and highly reproducible device. One of the sensors reported presents a typical resistive behaviour from 40% RH up to 85% RH with a sensitivity of -0.21 ($Z/\%RH$). The performance of the sensors obtained with several fabrication techniques is studied and reported at multiple frequencies from 100 Hz to 10 MHz, showcasing its versatility and robustness.

Keywords: moisture content, PEDOT:PSS, screen printing, biodegradable, NaCl

INTRODUCTION

Monitoring environmental variables is gaining relevance in key trend technologies like the Internet of Things (IoT) (Bouzebrak et al., 2019). For instance, controlling humidity is fundamental for developing IoT solutions like smart food packaging and environmental control systems for industrial and manufacturing processes (Najeeb et al., 2018). In this context, fabrication of flexible and thin-film humidity sensors is an important field of research in terms of device portability and compatibility. To ensure the reproducibility and accuracy during the fabrication process, stability control of the surrounding atmosphere is one of the main issues to deal with (Chen and Lu, 2005).

A humidity sensor is characterized by several parameters such as sensitivity, temperature dependence, and lesser hysteresis (Najeeb et al., 2018). Flexible humidity sensors reduce device dimensions, to adapt them to more complex design, while at the same time decreasing the cost of fabrication. Unfortunately, the task is not trivial. In fact, the fabrication of a flexible humidity sensor with satisfying performance in a wide range of humidities and temperatures has become an important goal in the literature (Chen and Lu, 2005). In addition, characterizing the device performance at different frequencies is essential to differentiate between its capacitive and resistive behavior at several frequencies, to establish its range of operation and to integrate it into a more complex sensor.

For humidity control of the environment, the amount of water in gas needs to be determined (ICEweb, 2015). In this respect, relative humidity (RH) is defined as the ratio of the partial pressure of water in gas to the saturation vapor pressure of a gas at a given temperature, and it is one of the most commonly used values for high humidity ranges. A wide variety of fabrication processes for humidity sensors are reported in literature (da Costa and Choi, 2020; Delipinar et al., 2021). Inkjet and screen-printing processing techniques are well standardized as mass fabrication techniques (Molina-Lopez et al., 2012; Zhang et al., 2018; Zhou et al., 2020). Spray coating is another approach employed in literature in the fabrication of humidity sensors (Lipomi et al., 2011; Kim and Yun, 2013; Bu et al., 2016; Kim et al., 2018). Also, drop casting method is reported as one of the simplest fabrication techniques for humidity sensors (Wei et al., 2019; Wu et al., 2019). The range of possible materials to be employed for humidity sensing purposes spans from ceramics, such as Al_2O_3 (Chakraborty et al., 1999), TiO_2 (Morimoto et al., 1969; McCafferty and Zettlemoyer, 1971), SiO_2 (Lin et al., 1993; D'apuzzo et al., 2000; Kong et al., 1997), and spinel compounds, to modified polyelectrolytes (Rauen et al., 1993; Sakai et al., 1995; Gong et al., 2002a; Gong et al., 2002b; Lee et al., 2013) and conductive polymers (Macdiarmid, 1987). In addition, humidity sensors based on carbon materials such as carbon nanotubes (Han et al., 2012; Zhu et al., 2019), carbon ink (Duan et al., 2021), and graphene (Burman et al., 2016; Hassan et al., 2018; Park et al., 2018; Wan et al., 2018) have been previously reported in literature. A 2D rGO:MoS_2 based humidity sensor with a sensitivity of 0.973 in the range from 30–80% RH is reported (Adib et al., 2021). In addition, a GO-based potentiometric humidity sensor shows a sensitivity between 5–20 mV/% RH in a range from 20–90% RH (Lei et al., 2021). Furthermore, in order to improve their water-resistive behaviour, some polyelectrolytes humidity sensors based on alkali salts are reported (Sadaoka et al., 1988; Sakai et al., 2001; Su et al., 2006). Impedance analysis is really useful in order to compare the resistive and capacitive behaviour of the moisture sensors and it constitutes the main procedure to electrically characterize a humidity sensor in literature (D'apuzzo et al., 2000; Kong et al., 1997; Sakai et al., 1995; Gong et al., 2002a; Gong et al., 2002b; Sadaoka et al., 1988; Sakai et al., 2001; Su et al., 2006). Humidity sensors based on alkali salts have been reported with a linear impedance behaviour from 20% RH measured at 1 kHz and 30 °C (38). Also, a linear variation from 585 to 2.9 k Ω in the humidity range from 30 to 90%RH has been reported for moisture sensors based on two mutually reactive copolymers (Gong et al., 2002a). In addition, a textile humidity sensor based on metal-organic framework as a sensing layer is reported with a humidity range from 0.71–90% RH (Rauf et al., 2020). Developing biodegradable sensors is highly relevant so as to reduce electronics waste and CO_2 emissions. However, some of the device's residues might be toxins that can percolate through the Earth and contaminate the water and food we consume. Therefore, developing green electronics based on biodegradable and biocompatible materials, as well as green fabrication methods, benefits sustainable IoT development. There have been considerable

efforts in recent literature to show the feasibility, functionality, and performance of such green electronics devices (Jung et al., 2017; Gao et al., 2019; Lu et al., 2019). In addition to that, the specific case of biodegradable moisture sensors is even more sought by the technical and scientific literature, because of its potentially disruptive impact in healthcare and food industry, and at the same time some humidity sensors and respiration monitoring sensors based on green materials have already been reported (Güder et al., 2016; Zhu et al., 2019).

In this direction, we present in this work humidity sensors based on common salt (NaCl) as the sensing layer. The devices have been fabricated and characterized at different frequencies in order to evaluate their performance as a hybrid humidity sensor. Dip coating and spray coating are compared so as to analyze the influence of the fabrication techniques device throughput. The physical characterization of the fabricated devices are performed by a scanning electron microscope (SEM) and optical microscope images in order to study the deposition of the salt dissolution on different materials. The sensors reported in this work were manufactured with cost-effective and reproducible techniques, which involve entirely biodegradable materials providing environmentally friendly devices.

MATERIALS AND METHODS

Sensor Fabrication

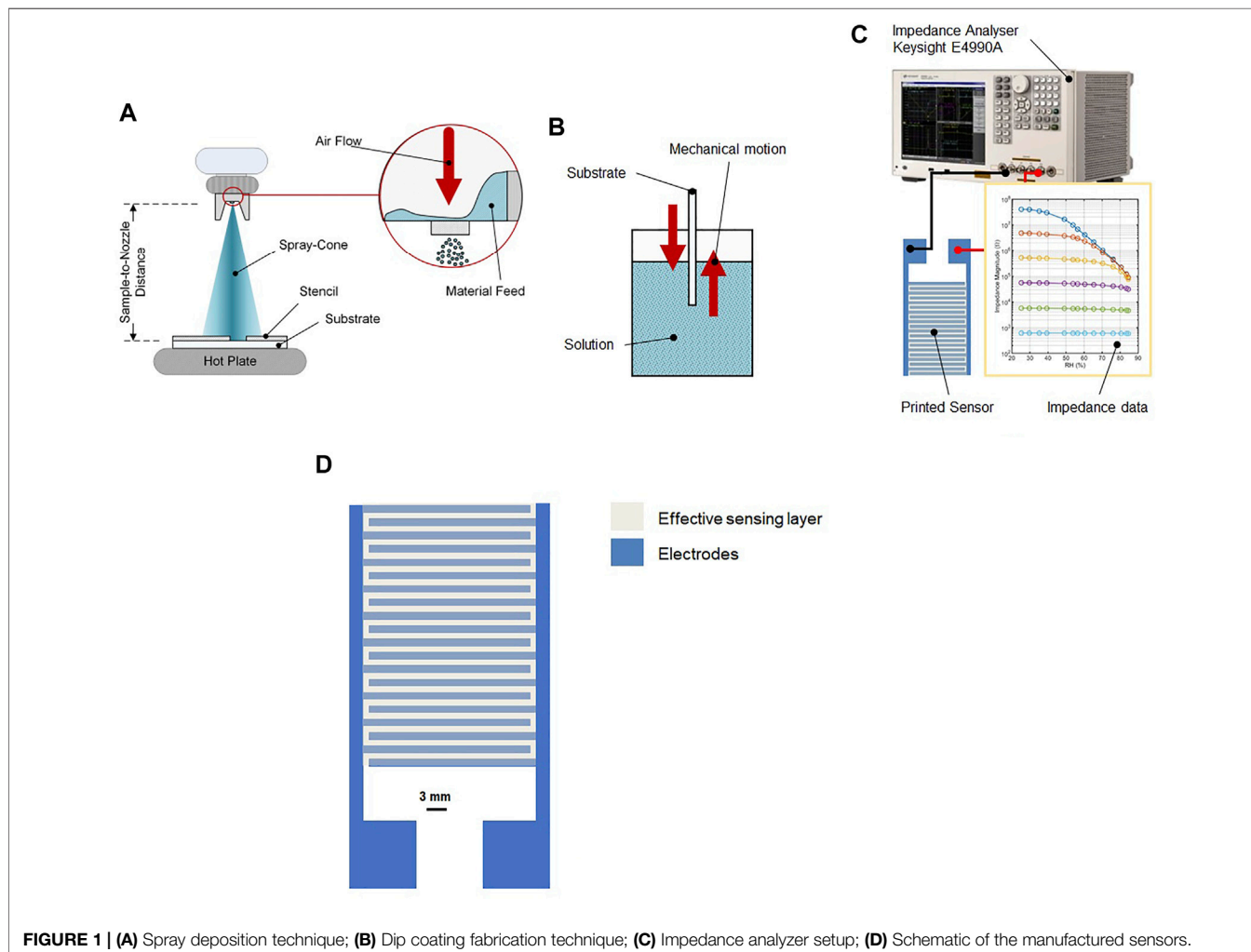
For the production of the sensors, two different substrates and two conductive pastes were employed. The common element of all the fabricated devices was the sensing layer: common kitchen salt (NaCl). In particular, we employed a solution made by dissolving 2 g NaCl in 10 ml of de-ionized water. While the solubility of NaCl in water is circa 3.6 g/10 ml (Haynes, 2014), we found it experimentally difficult to create a stable “ink”—especially in small batches—with more than 2.0 g/10 ml. Hence, the choice of the salt concentration was found empirically as the highest amount that would reliably not give any precipitation and be usable for multiple deposition sessions.

Such a solution was then deposited by means of spray coating and dip coating. Spray coating was carried out with a commercial airbrush. On fine setting, we deposited 4 ml of the salt solution over the IDEs with a uniform hand motion. The dip coating was performed by submerging the sensor in the solution for 2 min. The selected substrates were a bendable polyethylene terephthalate (PET) (Melinex[®] 506 from DuPont, Wilmington, DE, United States) and Whatman paper.

All sensors were manufactured by depositing first the sensing layer (see **Table 1** for deposition parameters) followed by the definition of the interdigitated electrodes (IDEs) by screen printing with a manual screen printer (Siebdruck Versand, Germany). **Figure 1A** and **Figure 1B** describe the two fabrication methods employed in the manufacturing of the sensors. In particular, interdigitated electrodes (IDE) were defined using a conductive paste made of poly (3,4-ethylenedioxythiophene) polystyrene sulfonate (PEDOT:PSS) at a weight content of 1.3 wt% (viscosity: >14,000 mPa s) (Sigma Aldrich, St. Louis, MO, United States). The drying of

TABLE 1 | Fabrication parameters.

Device	Deposition technique	Substrate	NaCl deposition parameters
Dip paper (Type 1)	Dip coating	Whatman paper	2 min then 70°C till dry
Type 2	Spray deposition	PET	4 ml at 70°C while spraying
Type 3	Spray deposition	PET	4 ml at 110°C while spraying



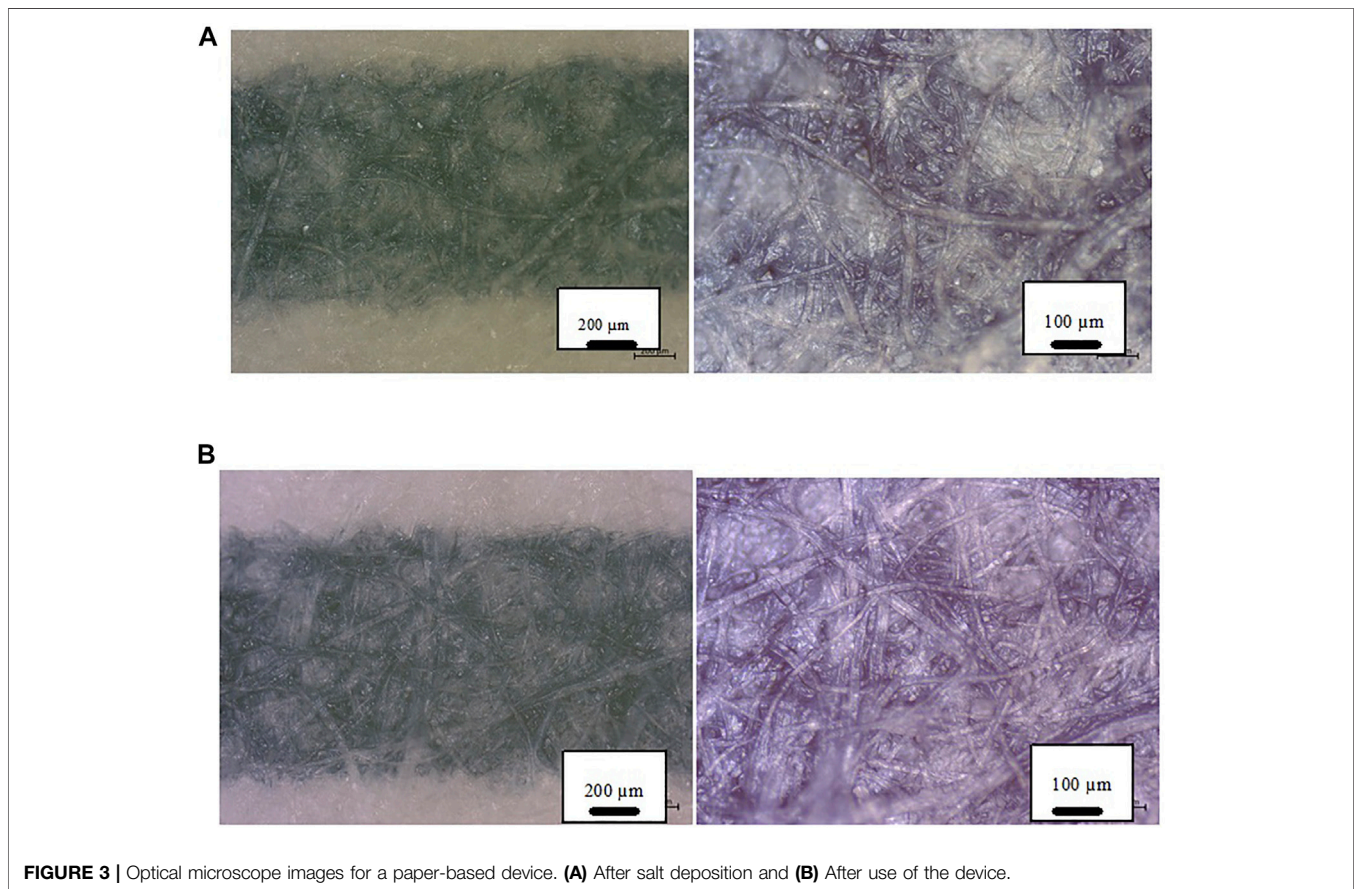
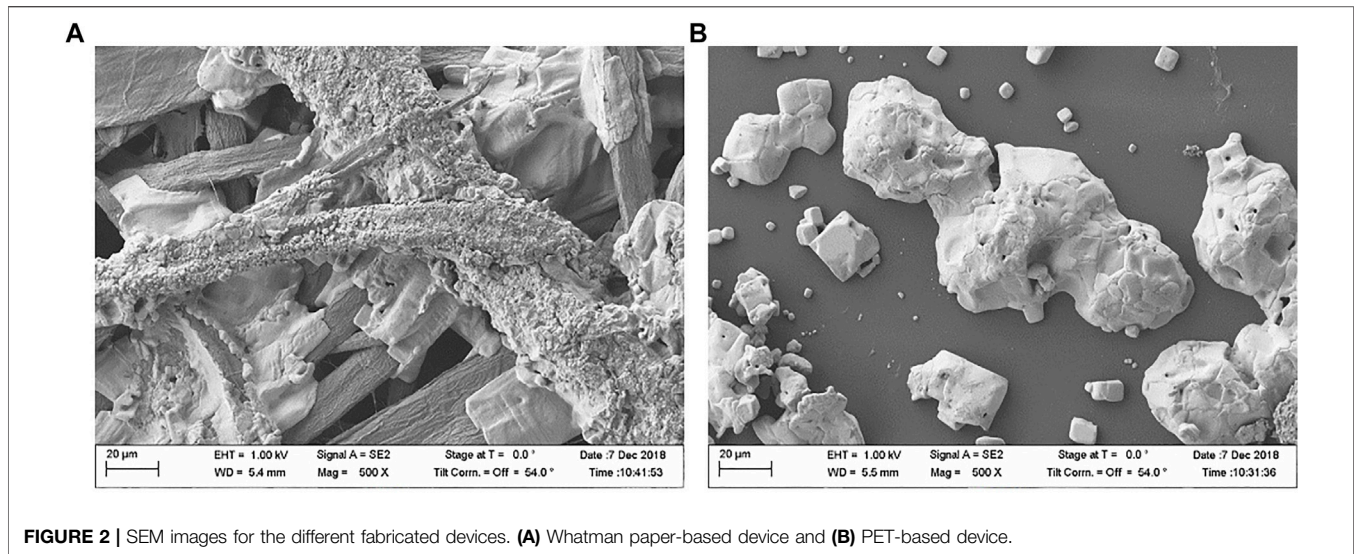
the conductive layer was done at 60°C for 10 min in a UF55 oven from Memmert (Schwabach, Germany). A schematic of the fabricated devices is shown in **Figure 1D**, highlighting the sensor's dimensions. The layout was selected following a previous design (Falco et al., 2021) to ensure proper definition of the IDE fingers, avoiding short circuits, and ensuring connectivity.

Characterization

In order to characterize the layers, sensor optical microscope images were taken with an Axiolab A1 MAT equipped with an Axiocam 105 color camera, both of Carl Zeiss AG (Germany). Field-emission scanning electron microscope (FESEM) images

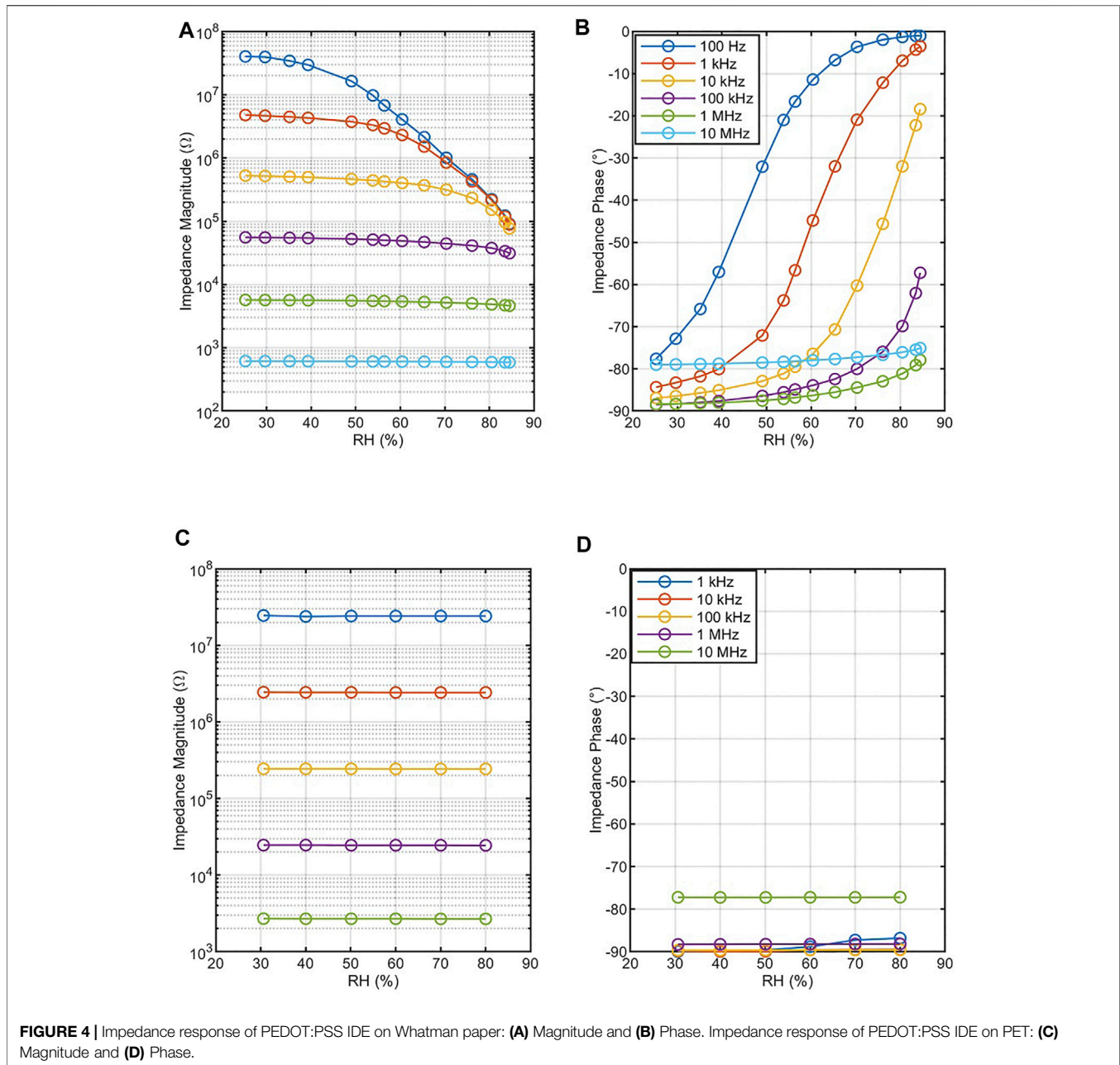
were recorded using an NVision40 from Carl Zeiss (Germany) at an acceleration voltage of 7.0 kV and an extraction voltage of 5.0 kV. In addition, scanning electron microscope (SEM) images were taken with an NVision40 of Carl Zeiss (Germany) at 5.0 kV beam energy and a magnification of 25,000.

In order to characterize the performance of the device in frequency, LabVIEW 2016 was used to automate the electrical measurements (see **Figure 1C** where the characterization setup is detailed). This software controls an impedance analyzer (Keysight E4990 A) that uses an impedance probe kit (42941 A) for the sensor readout. To perform the electrical measures a SubMiniature version A (SMA) male connector



was glued to the end points of the electrodes using silver paste. The excitation voltage applied in all measurements was $V_{DC} = 0$ and $V_{AC} = 500$ mV in the frequency range from 100 Hz to 10 MHz. In order to compensate the parasitic elements, a calibration was done before the measurements, just as in the one performed previously (Rivadeneira et al., 2014). The

temperature and humidity control were obtained placing the sensor in a climatic chamber (VLC4006) and the monitoring was performed over the climatic chamber sensor system. In order to ensure a stable value in the whole chamber volume for the RH sensing, the moisture content was ramped up in 10% steps and held for 1 h.



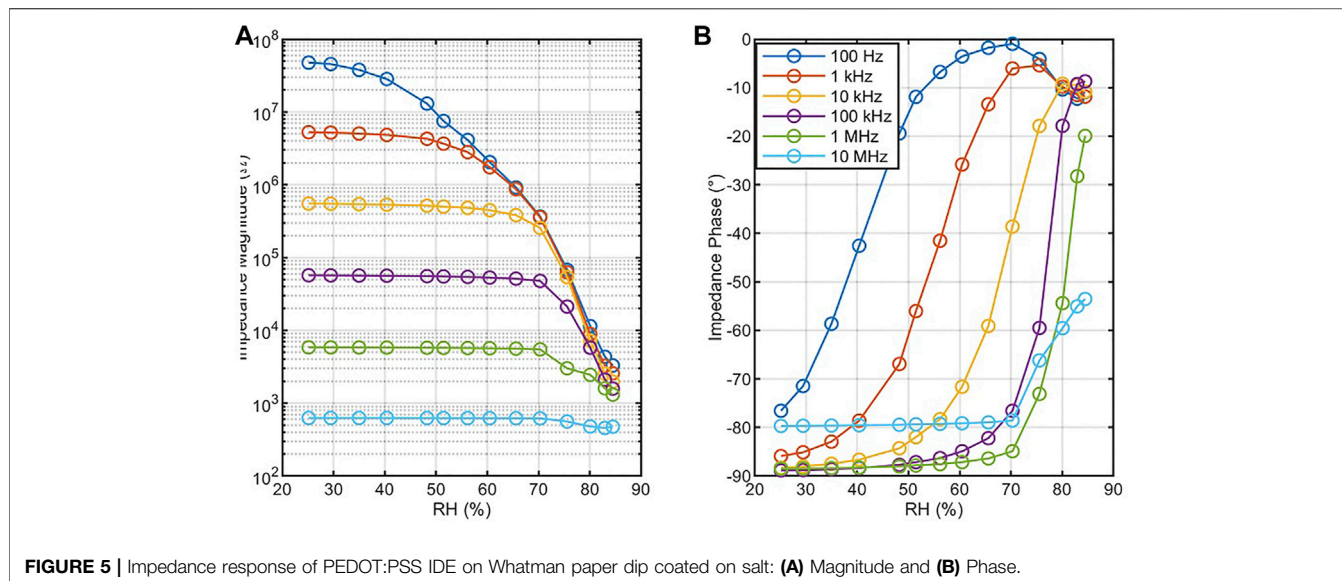
RESULTS AND DISCUSSION

Physical Characterization

In the following section the physical characterization of the devices is performed by the analysis of optical microscope and SEM images. **Figure 2** shows SEM images of the deposited salt layer on the fabricated devices for the different substrates used. It can be seen that for paper-based sensors the salt crystals are wrapped around the cellulose fibers, becoming part of the substrate itself, while for the devices manufactured on PET the salt agglomerates are on the substrate surface. The morphological properties of the Whatman paper induce a sort of “trapping” of the salt crystals, which are prone to remain in

their position even under stress. This is also found in the characterization of the devices: while PET-based devices lack measurement reproducibility, multiple measurement cycles on the paper substrate have shown significant change in the electrical characteristics.

To further confirm this point, we acquired optical microscope images of the paper-based humidity sensor **Figure 3** along its entire life-cycle: before and after salt deposition and after the use of the sensor. From the images, it can be observed that there is no significant optical change before and after using the devices, indicating that the salt crystals are still in place and can be reused multiple times.



Response to Moisture Content

Relative Humidity (RH) response of the device has been performed for a range of frequencies from 100 Hz up to 10 MHz. Deposition techniques of the sensing layer aforementioned in **Table 1** have been compared. The analysis of the impedance variation with relative humidity has been performed in order to study the magnitude and phase along the entire range of interest frequencies and its dependence with the substrate. **Figures 4A,B** shows the impedance characterization curves for a humidity sensor printed on Whatman paper without deposition of salt sensing layer. The magnitude and phase of the sensor impedance is measured for a range of relative humidity from 25 to 85% at 40°C.

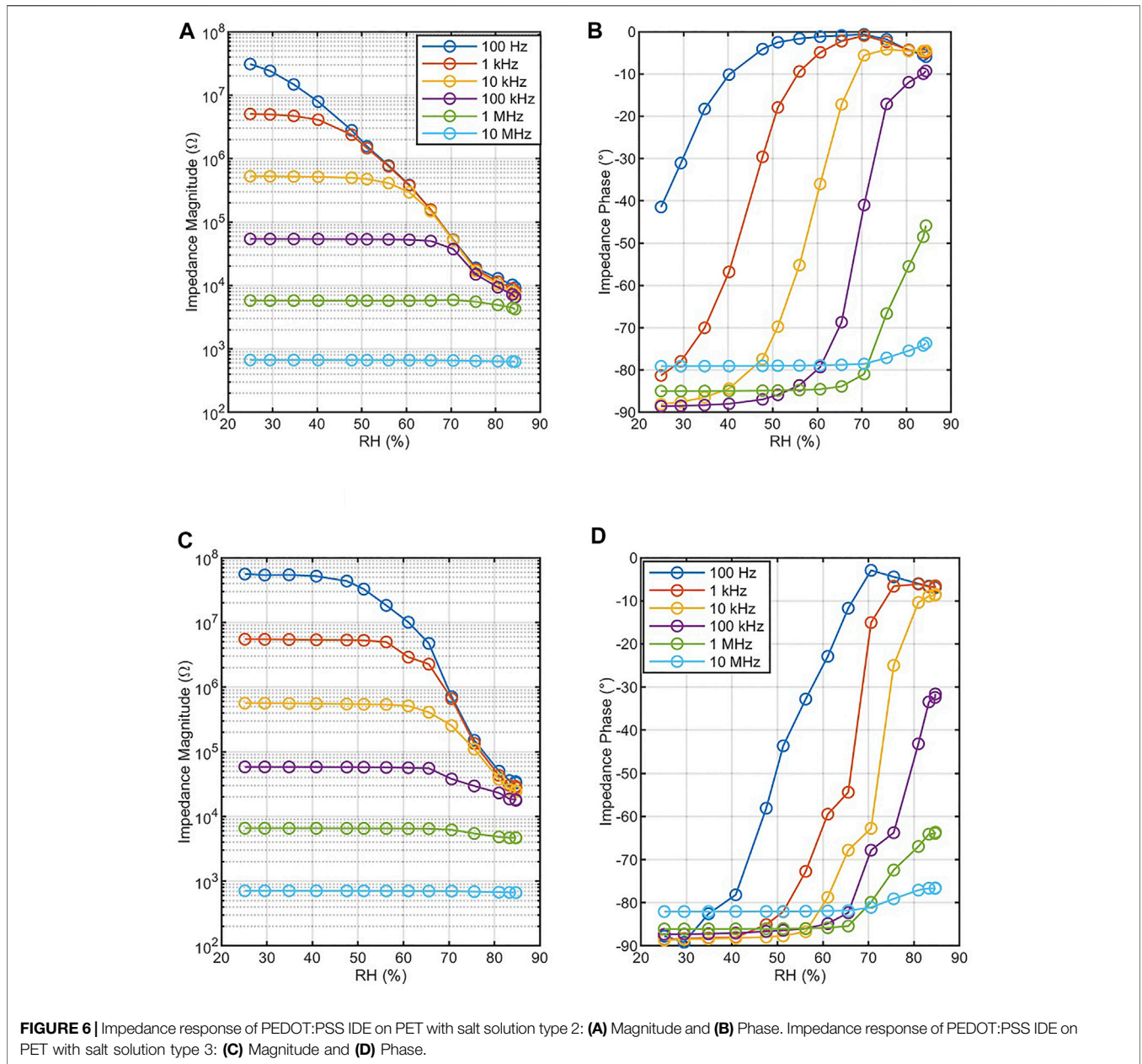
An increase of the magnitude of one order of magnitude per decade, as frequency falls, is evident from **Figure 4A**, consistent with a capacitive behavior. The magnitude response with RH is constant for the entire range of RH for 10 and 1 MHz. Nevertheless, as frequency decreases the magnitude becomes more sensitive to high RH. At 10 kHz, the magnitude starts falling at 50%RH, while for 100 Hz this behavior occurs at 30%RH. A phase increment as humidity grows is noted in **Figure 4B**. This variation of the phase is more pronounced as the frequency decreases. At 1 MHz phase varies from -88° up to 83° over the entire range of RH, however at 100 Hz this phase change significantly increases from -79° to -3° . These results confirm that at low frequencies, from 100 Hz to 10 kHz, the device presents a linear humidity response, which leads to a good performance as a capacitive humidity sensor. Nevertheless, as frequency increases the impedance response with respect to RH tends to stay constant.

The impedance characterization of PEDOT:PSS IDE on PET without any sensitive layer is shown in 4c and 4 days. The magnitude remains constant through the entire humidity range and the phase follows a similar behavior, showing a capacitive response in all cases. This last finding shows that the weak relationship between the impedance of the

paper-based sensor and the humidity must be related to the substrate itself and not to a variation of the electrodes' impedance—although PEDOT:PSS electrodes are partially water soluble. The IDE structure, however, is expected to behave as a humidity sensor as soon as it is covered with the salt solution. The underlying concept is that whenever the humidity increases, the salt will be dissolved in a superficial water layer. This layer will contain the dissolved salt and relative ions and will work as thin layer of standard saline solution, with a conductivity far greater than air's (Sauerheber and Heinz, 2015).

In these conditions, the conductive IDEs will not be bridged anymore by the high impedance air path, but they will be connected by a shallow conductive layer, Transforming the sensor from a capacitive structure to a mostly resistive one. Furthermore, this simple operating principle is based on a reversible physical reaction, which then ensures multiple operations and does not rely on any pre-treatment of the device before exposure.

To support this claim and to define it with precision, the impedance characterization of PEDOT:PSS IDE on Whatman paper dip coated on salt has been performed and shown in **Figure 5**. The effectiveness of the functionalization can only be judged on whether the salt treatment can expand the sensor's frequency response or not. As expected, the behavior at low humidity levels is purely capacitive, similar to what happened in the sensor without any functionalization. In this case, however, there is a significant difference when the device is exposed to higher RH levels and analyzed at higher frequencies. The PEDOT:PSS IDE on Whatman paper dip coated with salt presents better resistive humidity sensor behavior for higher RH values. At 1 MHz, the magnitude begins to decrease from $5.6\text{ k}\Omega$ all the way down to $1.3\text{ k}\Omega$ at RH of 70%, while for the device without the salt sensing layer the magnitude was constant in this frequency range. **Figure 5B** shows an increase of the phase at higher frequencies with respect to the device without dip-coating



functionalization. Furthermore, a decrement of the phase is noted for low frequencies at high RH in **Figure 5B**. A linear tendency is noted at low RH in magnitude, becoming exponential at higher RH. However, in phase a linear behavior in the entire range of RH overall at low frequencies is noted.

Figure 6C and **Figure 6D** show the impedance characterization of PEDOT:PSS IDE on PET with salt solution type 3. Similar to **Figure 4**, the magnitude and phase of the impedance changes as RH increases. The magnitude begins to decrease at 40%RH at 100 Hz unlike the PEDOT:PSS IDE on Whatman paper dip coated on salt, which shows this behavior at 25%RH at the same frequency. A similar phenomenon is observed at all frequencies, which causes the operation range to drift as frequency increases. The phase of the impedance shows

a similar drift of the operation range with respect to the frequency. **Figure 6D** denotes an operative range between 40% and 70%RH, while in **Figure 5B** this useful range was wider and comprised humidity values between 25% and 70%RH.

The fabrication method is not the only factor affecting the sensor's performance, as the processing parameters might also have an impact on it. The main parameters able to affect the deposition are the nozzle-to-substrate distance and the substrate temperature (Lavernia and Wu, 1996). The nozzle-to-substrate distance, however, also defines the area where it is possible to obtain a uniform deposition. The deposition cone originates at the orifice, and it is denser in its central sections with respect to its fringes. With a simple static setup like the one considered in this work—i.e., the airbrush is kept stable and there is no automated

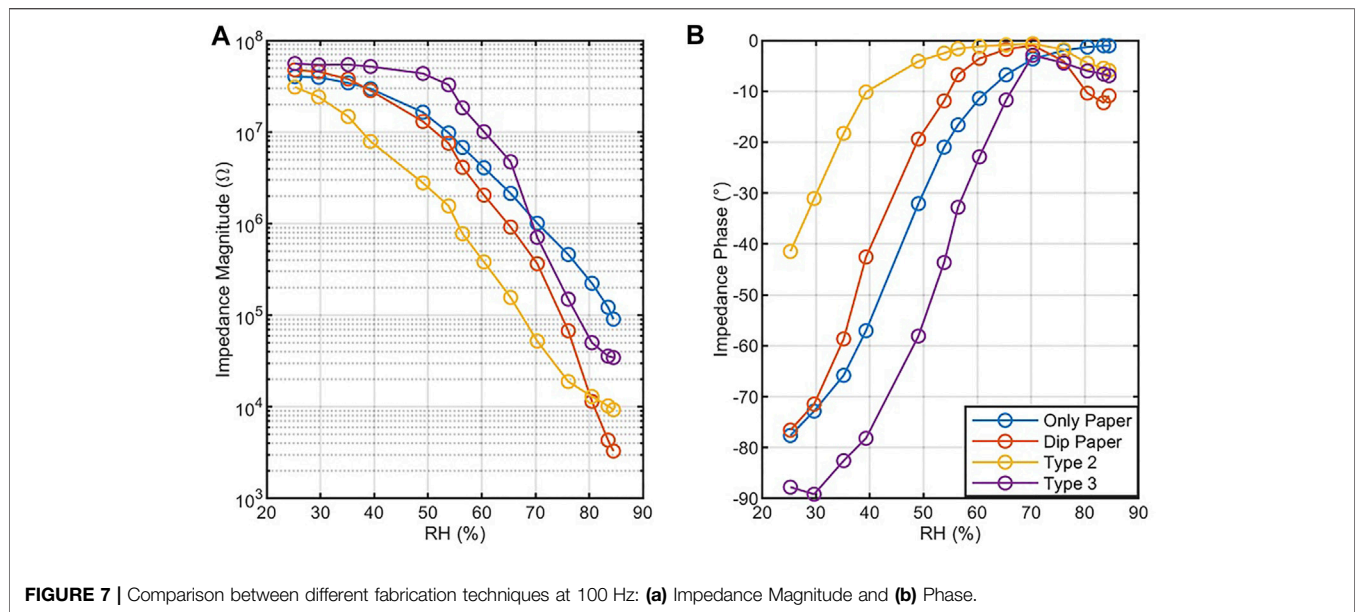


FIGURE 7 | Comparison between different fabrication techniques at 100 Hz: (a) Impedance Magnitude and (b) Phase.

TABLE 2 | RH range where the phase is linear and the regression parameters for each kind of fabricated device at 100 Hz.

Sensor type	Linear range in RH (%)	R ²	Slope (α/%RH)
Only paper	25.2–65.4	0.9852	1.96
Dip paper (Type 1)	25.1–56.2	0.9883	2.46
Spray coated Type 2	24.9–40.2	0.9887	2.08
Spray coated Type 3	34.9–70.6	0.9869	2.40

scanning motion—the distance is then dictated by the area of the sample. The remaining parameter that can play a significant role is then the temperature of deposition. A very high temperature allows for instant drying of the droplets, with the formation of a rough and reproducible layer. On the other extreme, a “wet” deposition allows for slow drying, which will assume patterns similar to “coffee stains”, leading to lower reproducibility. Operating in an “intermediate” regime allows for accurate layer control and for the formation of closed layers, which are smoother and extremely reproducible (Vak et al., 2007). In this context, we reduced the deposition temperature and proceeded with the impedance characterization for PEDOT:PSS IDE on PET with salt solution type 2, presented in Figure 6A and Figure 6B. The target temperature of 70 °C was found on the basis of previous works (Falco et al., 2015) and on an iteration process, as the lowest temperature at which it was possible to avoid wet layers. In this case, the range of operation as resistive humidity sensor, referent to the magnitude of the impedance, for 100 Hz covers all the humidity range characterized, between 25% and 85%RH. The phase of the impedance presents a shift of the operation range towards lower RH for frequencies up to 10 kHz where the curves tend to saturate. At 100 Hz the starting point of the phase is -41°, which provokes a lower saturation RH point at this frequency unlike the other devices.

Figure 7 presents a comparison, at 100 Hz, of the impedance for the different fabrication techniques used. A linearity study can be performed extracting the RH range where the phase is linear.

Table 2 summarizes the RH range for the phase linear zones together with the slope (sensitivity) and its linear coefficient (R²). All of the devices present a linear coefficient of circa 0.99. The device, which presents the largest RH linear range in phase, is the device without sensing layer deposition with RH range from 25.24% up to 65.36% RH. The device fabricated by dip coating shows the highest slope (2.46%/RH) but it also shows a limited linear range from 25.13% up to 56.16%. The device fabricated using spray type 3 shows the best compromise between the RH range, 34.87% up to 70.57% RH, and a slope of 2.40%/RH.

Table 3 presents some relevant points at 100 Hz from Figure 7. The magnitude conduction point represents the RH when the magnitude begins to decrease exponentially. The phase conduction point is defined as the RH value when the phase is near to -10° when reactance losses can be negligible and the sensor behavior can be modelled as a simple resistor. The spray type 2 technique reports a 24.95% RH at the beginning of the magnitude linear behavior and the phase is near -10° at 40% RH. Thus, this device can be modelled as a resistive sensor from 40%RH that is the lowest starting point of conduction measured for all the techniques at this frequency. The highest conduction point is reported by the spray technique type 3, since this presents a magnitude linear behavior at 47.54%RH and the phase shows a conduction point at 65%RH. Therefore, this device can be modelled as a purely resistive sensor from 65%RH. A wider range of resistive behavior is desirable, as it would allow for a simple design of the measuring electronics: if the sensor can be assimilated to a resistor, there is no need for measuring and elaborating complex impedance. Complexity, cost and ease of integration of resistive sensors are a clear advantage over their capacitive counterpart. The salt functionalization, hence, succeeds into expanding the “resistive range”, allowing for an inherently capacitive sensor (IDEs with no conductor in between) to be employed as a cost-effective resistive sensor.

In order to evaluate the outcome of our devices, Table 4 presents a comparison with some humidity sensor reported in literature. The

TABLE 3 | Magnitude and phase conduction points.

	Impedance magnitude conduction point		Impedance phase conduction point	
	Magnitude (M Ω)	RH (%)	Phase (ϕ)	RH (%)
Only paper	34.364	35.15	-11.41	60.40
Dip paper	37.923	34.97	-11.88	51.45
Type 2	30.092	24.95	-10.51	40.20
Type 3	43.518	47.54	-11.72	65.56

TABLE 4 | Comparison between different humidity sensors reported in literature. n.d. = not determined.

Materials	Fabrication	Output	RH	Flexible	Sensitivity	Ref
Poly (ionic liquids) on paper	Drop-casting	Impedance	11–95%	Yes	961.3 (Z _o /Z)	Zhao et al. (2018)
Nanofibrillated cellulose/MWCNTs composite film	TEMPO/NaClO/NaBr oxidation + mechanical homogenization	Current	11–95%	Yes	69% ($\Delta I/I_0$)	Zhu et al. (2019)
MWCNT + polyacrylic acid	Drop-casting	Resistance	30–90%	Yes	-0.15 (Z/%RH)	Lee et al. (2013)
PMMA + salt	Dip-coating	Impedance	20–90%	No	-0.03 (log Z/%RH)	Su et al. (2006)
	Dip-coating (Type 1)		48–84%	Yes	-0.23 (Z/%RH)	This work
			25–56%		2.46 (ϕ /RH)	
NaCl on paper	Spray-coating Type 2	Impedance	25–85%		-0.14 (Z/%RH)	
			25–40%		2.08 (ϕ /RH)	
	Spray-coating Type 3		48–85%		-0.21 (Z/%RH)	
			35–71%		2.40 (ϕ /RH)	

Type 2 sensor shows a good operation range for impedance magnitude compared to other devices in **Table 4**. Among the impedance-based sensors, our spray coated Type 2 device presents a comparable sensitivity with the PMMA and salt-based sensor (Su et al., 2006). Regarding fabrication techniques, spray-coating process employed in our sensor is more reproducible than the others techniques presented in **Table 4**. Regarding the low-cost commercial humidity sensors, products with a humidity range from 20 to 90% RH can be found (Multicomp, 2019; MulticompPRO, 2021). In addition, a humidity sensor with an operating range from 0 to 100% RH with a resolution of 0.03% RH can be found (I. S. Technology, 2016). There are also humidity sensors based on a capacitive response, a sensitivity of 0.31 ΔC /RH in a humidity range from 33 to 75% RH (T. connectivity, 2021). In conclusion, Type 2 sensor presents an outcome comparable with others sensor reported in literature, which also presents an easy fabrication method with cost-effective processes and biodegradable materials. Notice that the main drawback to the sensors realized on PET with spray deposited sensing layer is the adhesion of the film to the substrate without employing any binder. In the case of the dip coated ones, however, the sensing layer is attached to the paper fibers, leading to a robust layer. Nevertheless, even if the sensor on PET might be impaired if incorrectly manipulated, it can certainly still be used in applications where the sensing film and the electronic components are not expected to be touched.

CONCLUSIONS

Flexible humidity sensors based in a common salt (NaCl) sensing layer have been reported with a typical resistive behavior from 40% RH up to 85% RH at 100 Hz. A study of several fabrication techniques has been studied, such as dip coating and spreading

by spray at different frequencies. Using common salt in moisture sensors provide a low-cost and highly reproducible device, able to function in a wide resistive regime, which yields ease of integration in simple sensing nodes. All the fabrication process proposed in this paper are feasible and widely accessible. In addition, this is a fully biodegradable sensor since all the materials employed (paper-based substrate and salt as a sensing layer) and the fabrication techniques are environmentally friendly. Nowadays, the use of biodegradable, low-cost, and effective thin-film humidity sensors is fundamental to develop novel applications promoting sustainable development in a practicable way.

DATA AVAILABILITY STATEMENT

The raw data supporting the conclusion of this article will be made available by the authors, without undue reservation.

AUTHOR CONTRIBUTIONS

AF, Conceptualization, Validation, Writing-Review; Editing AM-S: Investigation, Formal analysis, Writing-Original draft FL: Conceptualization, Investigation EC: Resources AS-C: Supervision JS: Methodology, Writing-Review; Editing AR: Conceptualization, Supervision, Visualization, Funding acquisition, Writing-Original draft.

FUNDING

This work was funded by the fellowship H2020-MSCA-IF-2017-794885-SELFSENS. This work was partially funded by the

regional projects: B-RNM-680-UGR20, P20_00265 and the Spanish Ministry of Sciences and Innovation through the

National Project PID2020-117344RB-I00 and the Ramón y Cajal fellow RYC2019-027457-I.

REFERENCES

- Adib, M. R., Lee, Y., Kondalkar, V. V., Kim, S., and Lee, K. (2021). A Highly Sensitive and Stable rGO:MoS₂-Based Chemiresistive Humidity Sensor Directly Insertable to Transformer Insulating Oil Analyzed by Customized Electronic Sensor Interface. *ACS Sens.* 6 (3), 1012–1021. doi:10.1021/acssensors.0c02219
- Bouzembrak, Y., Klüchke, M., Gavai, A., and Marvin, H. J. (2019). Internet of Things in Food Safety: Literature Review and a Bibliometric Analysis. *Trends Food Sci. Tech.* 94, 54–64. doi:10.1016/j.tifs.2019.11.002
- Bu, Q., Zhan, Y., He, F., Lavorgna, M., and Xia, H. (2016). Stretchable Conductive Films Based on Carbon Nanomaterials Prepared by spray Coating. *J. Appl. Polym. Sci.* 133 (15). doi:10.1002/app.43243
- Burman, D., Ghosh, R., Santra, S., and Guha, P. K. (2016). Highly Proton Conducting MoS₂/graphene Oxide Nanocomposite Based Chemoresistive Humidity Sensor. *RSC Adv.* 6 (62), 57424–57433. doi:10.1039/c6ra11961a
- Chakraborty, S., Nemoto, K., Hara, K., and Lai, P. T. (1999). Moisture Sensitive Field Effect Transistors Using Gate Structure. *Smart Mater. Struct.* 8 (2), 274–277. doi:10.1088/0964-1726/8/2/014
- Chen, Z., and Lu, C. (2005). Humidity Sensors: a Review of Materials and Mechanisms. *Sen Lett.* 3 (4), 274–295. doi:10.1166/sl.2005.045
- D'apuzzo, M., Aronne, A., Esposito, S., and Pernice, P. (2000). Sol-gel Synthesis of Humidity-Sensitive P2O₅-SiO₂ Amorphous Films. *J. sol-gel Sci. Technol.* 17 (3), 247–254. doi:10.1023/a:1008720223563
- da Costa, T. H., and Choi, J. W. (2020). Fabrication and Patterning Methods of Flexible Sensors Using Carbon Nanomaterials on Polymers. *Adv. Intell. Syst.* 2 (5), 1900179. doi:10.1002/aisy.201900179
- Delipinar, T., Shafique, A., Gohar, M. S., and Yapici, M. K. (2021). Fabrication and Materials Integration of Flexible Humidity Sensors for Emerging Applications. *ACS omega* 6 (13), 8744–8753. doi:10.1021/acsomega.0c06106
- Duan, Z., Jiang, Y., Zhao, Q., Huang, Q., Wang, S., Zhang, Y., et al. (2021). Daily Writing Carbon Ink: Novel Application on Humidity Sensor with Wide Detection Range, Low Detection Limit and High Detection Resolution. *Sensors Actuators B: Chem.* 339, 129884. doi:10.1016/j.snb.2021.129884
- Falco, A., Sackenheim, P. S., Romero, F. J., Becherer, M., Lugli, P., Salmerón, J. F., et al. (2021). Fabrication of Low Cost and Low Impact RH and Temperature Sensors for the Internet of Environmental-Friendly Things. *Mater. Sci. Eng. B* 267, 115081. doi:10.1016/j.mseb.2021.115081
- Falco, A., Zaidi, A. M., Lugli, P., and Abdellah, A. (2015). Spray Deposition of Polyethylenimine Thin Films for the Fabrication of Fully-Sprayed Organic Photodiodes. *Org. Elect.* 23, 186–192. doi:10.1016/j.orgel.2015.05.003
- Gao, L., Zhu, C., Li, L., Zhang, C., Liu, J., Yu, H.-D., et al. (2019). All Paper-Based Flexible and Wearable Piezoresistive Pressure Sensor. *ACS Appl. Mater. Inter.* 11 (28), 25034–25042. doi:10.1021/acsmi.9b07465
- Gong, M.-S., Joo, S.-W., and Choi, B.-K. (2002). Humidity Sensor Using Mutually Reactive Copolymers Containing Quaternary Ammonium Salt and Reactive Function. *Sensors Actuators B: Chem.* 86 (1), 81–87. doi:10.1016/s0925-4005(02)00151-x
- Gong, M.-S., Joo, S.-W., and Choi, B.-K. (2002). Humidity-sensitive Properties of a Cross-Linked Polyelectrolyte Prepared from Mutually Reactive Copolymers. *J. Mater. Chem.* 12 (4), 902–906. doi:10.1039/b108647m
- Güder, F., Ainla, A., Redston, J., Mosadegh, B., Glavan, A., Martin, T. J., et al. (2016). Paper-Based Electrical Respiration Sensor. *Angew. Chem. Int. Ed.* 55 (19), 5727–5732. doi:10.1002/anie.201511805
- Han, J.-W., Kim, B., Li, J., and Meyyappan, M. (2012). Carbon Nanotube Based Humidity Sensor on Cellulose Paper. *J. Phys. Chem. C* 116 (41), 22094–22097. doi:10.1021/jp3080223
- Hassan, G., Bae, J., Lee, C. H., and Hassan, A. (2018). Wide Range and Stable Ink-Jet Printed Humidity Sensor Based on Graphene and Zinc Oxide Nanocomposite. *J. Mater. Sci. Mater. Electron.* 29 (7), 5806–5813. doi:10.1007/s10854-018-8552-z
- Haynes, W. M. (2014). *CRC Handbook of Chemistry and Physics*. CRC Press.
- ICEweb (2015). *ICEweb*. Available at: http://www.iceweb.com.au/Analyzer/humidity_sensors.html.
- I. S. Technology (2016). *HYT 271*.
- Jung, Y. H., Zhang, H., Gong, S., and Ma, Z. (2017). High-performance green Semiconductor Devices: Materials, Designs, and Fabrication. *Semicond. Sci. Technol.* 32 (6), 063002. doi:10.1088/1361-6641/aa6f88
- Kim, D., and Yun, K.-S. (2013). Patterning of Carbon Nanotube Films on PDMS Using SU-8 Microstructures. *Microsyst Technol.* 19 (5), 743–748. doi:10.1007/s00542-012-1677-8
- Kim, H., Park, S., Park, Y., Choi, D., Yoo, B., and Lee, C. S. (2018). Fabrication of a Semi-transparent Flexible Humidity Sensor Using Kinetically Sprayed Cupric Oxide Film. *Sensors Actuators B: Chem.* 274, 331–337. doi:10.1016/j.snb.2018.07.127
- Kong, L. B., Zhang, L. Y., and Yao, X. (1997). Preparation and Properties of a Humidity Sensor Based on LiCl-Doped Porous Silica. *J. Mater. Sci. Lett.* 16 (10), 824–826. doi:10.1023/a:1018534626228
- Lavernia, E. J., and Wu, Y. (1996). *Spray Atomization and Deposition*. Wiley-Blackwell.
- Lee, J., Cho, D., and Jeong, Y. (2013). A Resistive-type Sensor Based on Flexible Multi-Walled Carbon Nanotubes and Polyacrylic Acid Composite Films. *Solid-State Elect.* 87, 80–84. doi:10.1016/j.sse.2013.05.001
- Lei, D., Zhang, Q., Liu, N., Su, T., Wang, L., Ren, Z., et al. (2021). Self-Powered Graphene Oxide Humidity Sensor Based on Potentiometric Humidity Transduction Mechanism. *Adv. Funct. Mater.*, 2107330. doi:10.1002/adfm.202107330
- Lin, J., Heurich, M., and Obermeier, E. (1993). Manufacture and Examination of Various Spin-On Glass Films with Respect to Their Humidity-Sensitive Properties. *Sensors Actuators B: Chem.* 13 (1-3), 104–106. doi:10.1016/0925-4005(93)85335-8
- Lipomi, D. J., Vosgueritchian, M., Tee, B. C.-K., Hellstrom, S. L., Lee, J. A., Fox, C. H., et al. (2011). Skin-like Pressure and Strain Sensors Based on Transparent Elastic Films of Carbon Nanotubes. *Nat. Nanotech* 6 (12), 788–792. doi:10.1038/nnano.2011.184
- Lu, D., Liu, T. L., Chang, J. K., Peng, D., Zhang, Y., Shin, J., et al. (2019). Transient Light-Emitting Diodes Constructed from Semiconductors and Transparent Conductors that Biodegrade under Physiological Conditions. *Adv. Mater.* 31 (42), 1902739. doi:10.1002/adma.201902739
- Macdiarmid, A. G. (1987). Conducting Polymers: What Does the Future Hold? *Synth. Met.* 21 (1-3), 79–83. doi:10.1016/0379-6779(87)90069-5
- McCafferty, E., and Zettlemoyer, A. C. (1971). Adsorption of Water Vapour on α -Fe₂O₃. *Discuss. Faraday Soc.* 52, 239–254. doi:10.1039/d1f9715200239
- Molina-Lopez, F., Briand, D., and de Rooij, N. F. (2012). All Additive Inkjet Printed Humidity Sensors on Plastic Substrate. *Sensors Actuators B: Chem.* 166–167, 212–222. doi:10.1016/j.snb.2012.02.042
- Morimoto, T., Nagao, M., and Tokuda, F. (1969). Relation between the Amounts of Chemisorbed and Physisorbed Water on Metal Oxides. *J. Phys. Chem.* 73 (1), 243–248. doi:10.1021/j100721a039
- Multicomp (2019). *Humidity Sensor*.
- MulticompPRO (2021). *Humidity Sensors*.
- Najeeb, M. A., Ahmad, Z., and Shakoore, R. A. (2018). Organic Thin-Film Capacitive and Resistive Humidity Sensors: A Focus Review. *Adv. Mater. Inter.* 5 (21), 1800969. doi:10.1002/admi.201800969
- Park, S. Y., Kim, Y. H., Lee, S. Y., Sohn, W., Lee, J. E., Kim, D. H., et al. (2018). Highly selective and sensitive chemoresistive humidity sensors based on rGO/MoS₂ van der Waals composites. *J. Mater. Chem. A* 6 (12), 5016–5024. doi:10.1039/c7ta11375g
- Rauen, K. L., Smith, D. A., Heineman, W. R., Johnson, J., Seguin, R., and Stoughton, P. (1993). Humidity Sensor Based on Conductivity Measurements of a Poly(dimethyldiallylammonium Chloride) Polymer Film. *Sensors Actuators B: Chem.* 17 (1), 61–68. doi:10.1016/0925-4005(93)85184-c
- Rauf, S., Vijjapu, M. T., Andrés, M. A., Gascón, I., Roubeau, O., Eddaoudi, M., et al. (2020). Highly Selective Metal-Organic Framework Textile Humidity Sensor. *ACS Appl. Mater. Inter.* 12 (26), 29999–30006. doi:10.1021/acsmi.0c07532

- Rivadeneira, A., Fernández-Salmerón, J., Agudo, M., López-Villanueva, J. A., Capitan-Vallvey, L. F., and Palma, A. J. (2014). Design and Characterization of a Low thermal Drift Capacitive Humidity Sensor by Inkjet-Printing. *Sensors Actuators B: Chem.* 195, 123–131. doi:10.1016/j.snb.2013.12.117
- Sadaoka, Y., Matsuguchi, M., Sakai, Y., and Takahashi, K. (1988). Effects of Sorbed Water on the Dielectric Constant of Some Cellulose Thin Films. *J. Mater. Sci. Lett.* 7 (2), 121–124. doi:10.1007/bf01730591
- Sakai, Y., Matsuguchi, M., and Yonesato, N. (2001). Humidity Sensor Based on Alkali Salts of Poly (2-Acrylamido-2-Methylpropane Sulfonic Acid). *Electrochimica acta* 46 (10-11), 1509–1514. doi:10.1016/s0013-4686(00)00746-5
- Sakai, Y., Sadaoka, Y., Matsuguchi, M., and Sakai, H. (1995). Humidity Sensor Durable at High Humidity Using Simultaneously Crosslinked and Quaternized Poly (Chloromethyl Styrene). *Sensors Actuators B: Chem.* 25 (1-3), 689–691. doi:10.1016/0925-4005(95)85152-6
- Sauerheber, R., and Heinz, B. (2015). Temperature Effects on Conductivity of Seawater and Physiologic saline, Mechanism and Significance. *Chem. Sci. J.* 6, 109.
- Su, P.-G., Sun, Y.-L., and Lin, C.-C. (2006). Humidity Sensor Based on PMMA Simultaneously Doped with Two Different Salts. *Sensors Actuators B: Chem.* 113 (2), 883–886. doi:10.1016/j.snb.2005.03.052
- T. connectivity (2021). *HS1101LF*.
- Vak, D., Kim, S.-S., Jo, J., Oh, S.-H., Na, S.-I., Kim, J., et al. (2007). Fabrication of Organic Bulk Heterojunction Solar Cells by a spray Deposition Method for Low-Cost Power Generation. *Appl. Phys. Lett.* 91 (8), 081102. doi:10.1063/1.2772766
- Wan, N., Wang, T., Tan, X.-y., Lu, S., Zhou, L.-l., Huang, J.-q., et al. (2018). Microstructure Related Synergic Sensing Mechanism in Graphene Oxide Humidity Sensor. *J. Phys. Chem. C* 122 (1), 830–838. doi:10.1021/acs.jpcc.7b09744
- Wei, Y., Qiao, Y., Jiang, G., Wang, Y., Wang, F., Li, M., et al. (2019). A Wearable Skinlike Ultra-sensitive Artificial Graphene Throat. *ACS nano* 13 (8), 8639–8647. doi:10.1021/acsnano.9b03218
- Wu, J., Sun, Y.-M., Wu, Z., Li, X., Wang, N., Tao, K., et al. (2019). Carbon Nanocoil-Based Fast-Response and Flexible Humidity Sensor for Multifunctional Applications. *ACS Appl. Mater. Inter.* 11 (4), 4242–4251. doi:10.1021/acsami.8b18599
- Zhang, R., Peng, B., and Yuan, Y. (2018). Flexible Printed Humidity Sensor Based on Poly(3,4-Ethylenedioxythiophene)/reduced Graphene oxide/Au Nanoparticles with High Performance. *Composites Sci. Tech.* 168, 118–125. doi:10.1016/j.compscitech.2018.09.013
- Zhao, H., Lin, X., Qi, R., Dai, J., Liu, S., Fei, T., et al. (2018). A Composite Structure of *In Situ* Cross-Linked Poly (Ionic Liquid) S and Paper for Humidity-Monitoring Applications. *IEEE Sensors J.* 19 (3), 833–837.
- Zhou, C., Zhang, X., Tang, N., Fang, Y., Zhang, H., and Duan, X. (2020). Rapid Response Flexible Humidity Sensor for Respiration Monitoring Using Nano-Confined Strategy. *Nanotechnology* 31 (12), 125302. doi:10.1088/1361-6528/ab5cda
- Zhu, P., Liu, Y., Fang, Z., Kuang, Y., Zhang, Y., Peng, C., et al. (2019). Flexible and Highly Sensitive Humidity Sensor Based on Cellulose Nanofibers and Carbon Nanotube Composite Film. *Langmuir* 35 (14), 4834–4842. doi:10.1021/acs.langmuir.8b04259

Conflict of Interest: The authors declare that the research was conducted in the absence of any commercial or financial relationships that could be construed as a potential conflict of interest.

Publisher's Note: All claims expressed in this article are solely those of the authors and do not necessarily represent those of their affiliated organizations, or those of the publisher, the editors, and the reviewers. Any product that may be evaluated in this article, or claim that may be made by its manufacturer, is not guaranteed or endorsed by the publisher.

Copyright © 2022 Falco, Marín-Sánchez, Loghin, Castillo, Salinas-Castillo, Salmerón and Rivadeneira. This is an open-access article distributed under the terms of the Creative Commons Attribution License (CC BY). The use, distribution or reproduction in other forums is permitted, provided the original author(s) and the copyright owner(s) are credited and that the original publication in this journal is cited, in accordance with accepted academic practice. No use, distribution or reproduction is permitted which does not comply with these terms.